Engineering Analysis with Boundary Elements 33 (2009) 731–740

Contents lists available at ScienceDirect

Engineering Analysis with Boundary Elements

journal homepage: www.elsevier.com/locate/enganabound

Poroelastic analysis of bone tissue differentiation by using the boundary element method

Y. González [a,*], M. Cerrolaza [a], C. González [b]

[a] Instituto Nacional de Bioingeniería, Facultad de Ingeniería, Universidad Central de Venezuela, Caracas, Venezuela
[b] Servicio de Traumatología y Ortopedia, Hospital Universitario de Caracas, Caracas, Venezuela

ARTICLE INFO

Article history:
Received 25 February 2008
Accepted 22 September 2008
Available online 29 November 2008

Keywords:
Bone healing
Tissue differentiation
Boundary element method
Poroelasticity
Axi-symmetry

ABSTRACT

Fracture healing is initiated and tightly regulated mainly by growth factors and by mechanical environment around the callus site. Biomechanics of fracture healing have been previously studied. Most computational models are based on finite elements and some of them study the level of strain or stress in the different tissues. These strain/stress fields are the main mechanical stimuli affecting cell differentiation and ossification pathway. In this work, we incorporated that hypothesis into a poroelastic axi-symmetric boundary element callus model, where the pore pressure was included as a part of the stimuli function. This analysis allowed us to extend the observations made by other authors and a new poroelastic correlation between mechanical conditions and local tissue formation is proposed. This work shows the capability of the boundary element method to characterize the tissue phenotypes during a progressive healing process. The results were in good agreement with those reported in previous works.

1. Introduction

1.1. Bone healing and tissue regeneration

Once a fracture occurs, a very complex process is auto-activated naturally to repair the injury. Fracture healing involves the generation of intermediate tissues, such as fibrous connective tissue, cartilage and woven bone, before final bone healing can occur, with different paths being governed by a variety of stimulating agents like the mechanical environment, hormonal and physiological patterns, geometric configuration of the fracture fragments and growth factors [1].

We can differentiate between primary or secondary fracture healing. However, most cases, which involve moderate gap sizes and fracture stability, heal by secondary fracture healing forming a voluminous callus. This type of healing benefits from a certain amount of inter-fragmentary movement (IFM) at the fracture site and has a series of sequential stages than can overlap to a certain extent, including inflammation, callus differentiation, ossification and remodelling. Bone ossification can occur mainly by endochondral and intramembranous ossification. In the first, cartilage is formed, calcified and replaced by bone. In the second, bone is formed directly by osteoblasts. As depicted in Fig. 1, the process involves the coordinated participation of migration, differentiation and proliferation of inflammatory cells, angioblasts, fibroblasts, chondroblasts and osteoblasts which synthesize and release bioactive substances of extracellular matrix components (e.g., different types of collagen and growth factors).

Healing begins as undifferentiated mesenchymal cells migrating from the surroundings to produce initial connective tissue around the fracture site, forming an initial stabilizing callus. These cells proliferate and migrate from the surrounding soft tissue.

In the next stage, the localized differentiation of the mesenchymal cells into cartilage and bone forming cells leads to the production of cartilage and bone tissue in the callus (see Fig. 2), depending on the biological and mechanical conditions. These differentiated cells begin to synthesize the extracellular matrix of their corresponding tissue. Intramembranous woven bone is produced by direct differentiation of the stem cells into osteoblasts and appears adjacent to each side of the gap site, advancing to the center of the callus. At the same time, at the center of the callus, cartilage is formed by chondrogenesis (Fig. 2), except right beside the gap where the stability is still very small and high relative displacement prevents the differentiation of mesenchymal cells.

Once the callus is filled (mainly by cartilage), endochondral ossification begins following a complex sequence of cellular events including cartilage maturation and degradation, vascularity and osteogenesis. The ossification continues until all the

* Corresponding author. Tel.: +58 212 8384868, +58 212 6051750/1751; fax: +58 212 6053115.
E-mail address: yomar.gonzalez@inabio.edu.ve (Y. González).

0955-7997/$ - see front matter © 2008 Elsevier Ltd. All rights reserved.
doi:10.1016/j.enganabound.2008.09.008

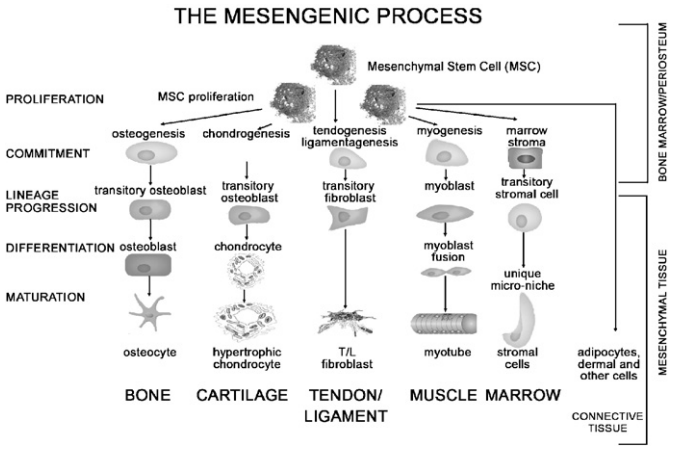

Fig. 1. The mesengenic process [3].

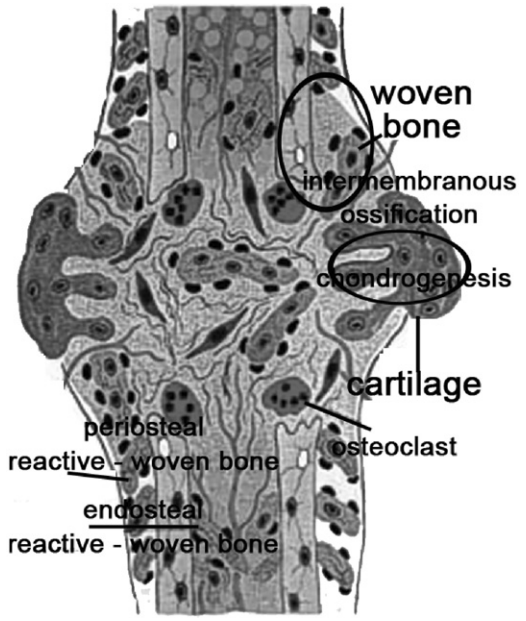

Fig. 2. Callus phenotype at day 9 after fracture. Notice the intramembranous ossification process close to the periosteum and the chondrogenesis present in most of fracture site [4].

cartilage has been replaced by bone and a bony bridge surrounds the fracture gap, achieving a good stabilization and sufficient stiffness. When the fracture is completely stabilized, mesenchymal cells start to invade the gap. Once the gap has ossified, remodelling of the fracture site begins gradually in order to restore the original internal structure and shape [2].

1.2. Boundary element framework

The boundary element method has recently been widely applied in simulation of biological problems. A few interesting works have been published illustrating the versatility of the method in this area [5–7].

The advantages below are believed to support the applicability of the method as a framework for bone healing simulation.

- High accuracy can be expected at the boundaries, internal points and interfaces from the strain/stress field magnitudes [5].
- Multi-domain capability [8].
- A generalized boundary integral equation for non-homogeneous isotropic media [9] can be applied within each region with spatially varying material properties.
- The BEM distinguishes itself as a boundary method, meaning that the numerical discretization is conducted at reduced spatial dimension [10].
- Remeshing is no longer needed to update callus size and shape.
- Kernels for time dependent analysis of diffusion and particles migration problems are available [11,12].
- No-symmetric boundary conditions have been incorporated into recent axi-symmetric kernels [13].
- Displacements and tractions at the boundaries can be calculated simultaneously.

The aim is therefore to establish BEM as an attractive alternative to the more familiar finite difference and finite element methods to characterize the strain/stress environment at appropriate locations within callus. The poroelastic code presented is part of a set of BEM codes needed to establish a dynamic callus growth model. All results were in good agreement with those reported in previous works, highlighting the potential of the axi-symmetric multi-region code to establish the mechanical stimuli associated with a specific tissue phenotype.

The BEM code contains the axi-symmetric fundamental solutions for steady-state poroelastic problems in a linear-elastic, isotropic and non-homogeneous media, following the Biot consolidation theory [14].

The constitutive equations for three-dimensional consolidation, written in the Cartesian form are

$$(\lambda+\mu)u_{j,i,j}+\mu u_{i,jj}-\beta p_{,i}+f_i=0 \tag{1}$$

$$kp_{,jj}-\left(\frac{\beta^2}{\lambda_u-\lambda}\right)\dot{p}-\beta\dot{u}_{j,j}+\psi=0 \tag{2}$$

where u_i represents the displacement, p is the excess pore pressure, f_i is the body force per unit volume, and ψ is the time rate of volumetric fluid supply per unit volume. Meanwhile, λ and μ are the drained Lamé elastic constants, λ_u is the undrained elastic modulus, k is the permeability and β is a function of B, called the compressibility coefficient or Skempton pore pressure coefficient.

The uncoupled poroelastic boundary integral equation for axi-symmetric bodies follows the matrix form (3). The generalized quasi-static displacements and tractions are transformed into a cylindrical coordinate system (r,φ,z) and then circuferential integration is performed. [15,16]

$$\begin{bmatrix} C_{rr}(P) & C_{rz}(P) & C_{r\theta}(P)\\ C_{zr}(P) & C_{zz}(P) & C_{z\theta}(P)\\ C_{\theta r}(P) & C_{\theta z}(P) & C_{\theta\theta}(P)\end{bmatrix}\begin{bmatrix} U_r(P)\\ U_z(P)\\ \theta(P)\end{bmatrix}$$
$$=2\pi\int_\Gamma\begin{bmatrix} U^*_{rr}(P,Q) & U^*_{rz}(P,Q) & U^*_{r\theta}(P,Q)\\ U^*_{zr}(P,Q) & U^*_{zz}(P,Q) & U^*_{z\theta}(P,Q)\\ U^*_{\theta r}(P,Q) & U^*_{\theta z}(P,Q) & U^*_{\theta\theta}(P,Q)\end{bmatrix}\begin{bmatrix} T_r(Q)\\ T_z(Q)\\ q(Q)\end{bmatrix}r(Q)\,d\Gamma$$
$$-2\pi\int_\Gamma\begin{bmatrix} T^*_{rr}(P,Q) & T^*_{rz}(P,Q) & T^*_{r\theta}(P,Q)\\ T^*_{zr}(P,Q) & T^*_{zz}(P,Q) & T^*_{z\theta}(P,Q)\\ T^*_{\theta r}(P,Q) & T^*_{\theta z}(P,Q) & T^*_{\theta\theta}(P,Q)\end{bmatrix}\begin{bmatrix} U_r(Q)\\ U_z(Q)\\ \theta(Q)\end{bmatrix}r(Q)\,d\Gamma \tag{3}$$

P is the field point, Q is the integration point, $C_{\alpha\eta}(P)$ is the free term, $r(Q)$ is the radial coordinate of Q, U_r and U_z are the displacements in radial and axial direction, respectively, θ is now called the excess pore pressure, T_r and T_z are the tractions in radial and axial direction, respectively. $U*_{rr}(P,Q)$, $U*_{rz}(P,Q)$, $U^*_{zr}(P,Q)$, $U^*_{zz}(P,Q)$, $T^*_{rr}(P,Q)$, $T^*_{rz}(P,Q)$, $T^*_{zr}(P,Q)$ and $T^*_{zz}(P,Q)$ are the kernel

functions identical to those of axi-symmetric elastic displacements and tractions [17,18]. Meanwhile, $U^*_{\theta\theta}$ and $T^*_{\theta\theta}$ are the potential flow axi-symmetric kernels [15,19]. $U^*_{r\theta}(P,Q)$, $U^*_{z\theta}(P,Q)$, $T^*_{r\theta}(P,Q)$ and $T^*_{z\theta}(P,Q)$, are the coupling terms [15,20]. The remaining components are zero due to the uncoupled theory considered.

2. Materials and methods

2.1. Quantitative tissue differentiation theory

The quantitative tissue differentiation theory proposed by Claes and Heigele [21] was a remarkable contribution to a better understanding of the complex fracture healing phenomenon. This work was used as a reference to support the methodology applied to obtain new results.

They hypothesized that new bone formation in fracture gap primarily occurs along the edges of existing bone or calcified tissue and that tissue phenotype depends on the local stress and strain magnitudes. Their quantitative algorithm specified limits for when intramembranous ossification or endochondral ossification would occur, as well as differentiation into fibrous tissue [22].

To describe progressive stiffening of the callus, the axi-symmetric finite element model (FEM) assumed five tissue types differing in their elastic material properties (Table 1). The tissue material properties were obtained from indentation tests on tissue sections from different callus regions [23]. The behavior of connective tissue was simulated using non-linear hyperelastic constitutive law, meanwhile all other tissue types were idealized as a linear-elastic. All materials were considered isotropic and homogeneous.

The FEM model assumed three different healing stages as depicted in Fig. 3, with 3 mm of osteotomy gap and 1.2 mm initial IFM, in a standardized transverse osteotomy of the right metatarsal of a group of sheep.

The study compares the global strain field and stresses (hydrostatic pressure) in the callus as calculated from the FEM simulation with histological data from a sheep fracture model. The temporal decrease of IFM was also studied (see Fig. 4).

The hypothesis predicts intramembranous bone formation for strains smaller than $\pm 5\%$ and hydrostatic pressures smaller than ± 0.15 MPa. Endochondral ossification is associated with compressive pressures larger than about -0.15 MPa and strains smaller than $\pm 15\%$. All other conditions seemed to lead to connective tissue or fibrous cartilage [21].

Table 1
Materials properties of the tissues considered [21].

Tissue type	Young's modulus (MPa)	Poisson ratio	Mooney–Rivlin constants
Initial connective tissue (ICT)	3	0.4	0.293
Soft callus (SOC)	1000	0.3	0.177
Intermediate stiffness callus (MSC)	3000	0.3	–
Stiff callus (SC)	6000	0.3	–
Chondroid ossification zone (COZ)	10,000	0.3	–
Cortex (C)	20,000	0.3	–
Fascie (F)	250	0.4	–

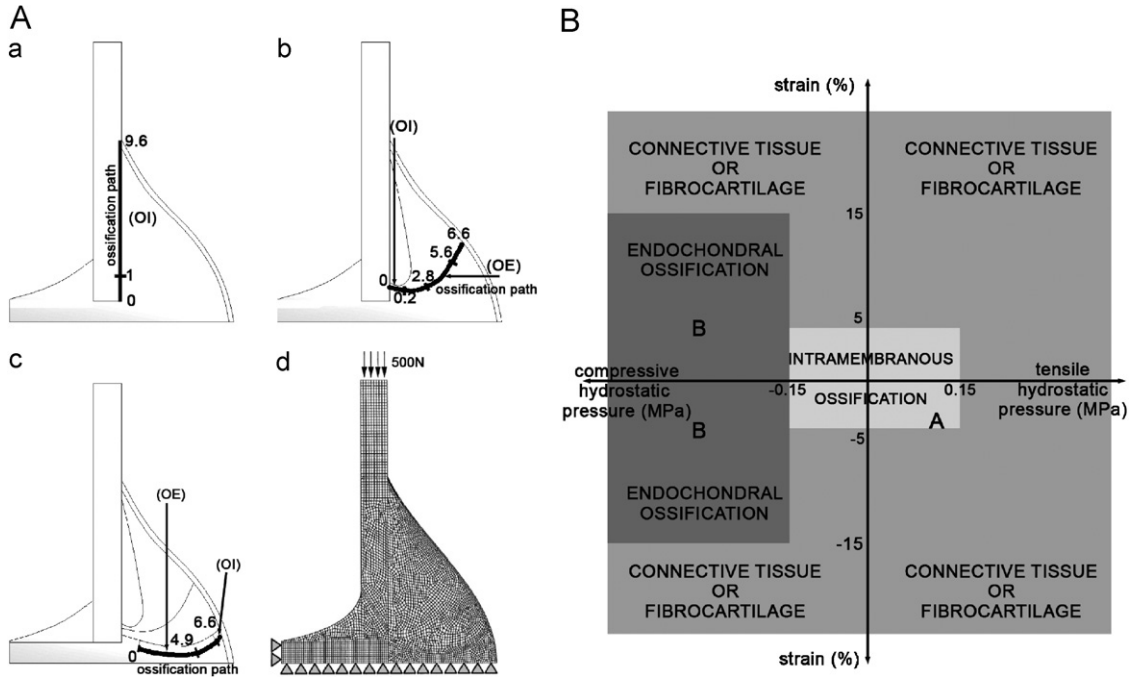

Fig. 3. (A) Axi-symmetric simulation of the three healing stages considered and the ossification paths: (a) 1 week p.o., (b) 4 weeks p.o., (c) 8 weeks p.o. and (d) FEM model and boundary conditions. (OI) surface of intramembranous ossification, (OE) surface of endochondral ossification. (B) Correlations between the mechanical conditions and types of tissue formed in the callus site as described by Claes and Heigele [21].

2.2. Course of inter-fragmentary movement (IFM)

Even if the bone fragments are stabilized, moderate axial movement in the range of 0.2–1.0 mm in gap sizes of 3 mm are believed to promote optimal healing in transverse osteotomies [24,25]. The influence of shear IFM on fracture healing remains a subject of controversy. Traditionally shear movements have been considered detrimental to healing, but recent experimental evidence has been contradictory [26,27]. However, once again, only axial displacement is considered to perform the analyses.

To be able to control the amount of IFM, the relationship between bony loading and fixation stiffness must be known all the time, to achieve sufficient mechanical stability in the newly formed bone [24].

To represent the optimal mechanical conditions at a fracture gap, that relationship was simplified. The loading history was assumed to be the same present in a sheep with an intact metatarsal [28,29].

Load cases (200–500 N) were applied by Claes et al. [21,30], under external fixator stabilization. The maximum IFM was reported for each consolidation stage as a function of strain conditions imposed. In this work, a loading of 500 N and 31% of inter-fragmentary strain (IFS) were considered, as depicted in Fig. 5a.

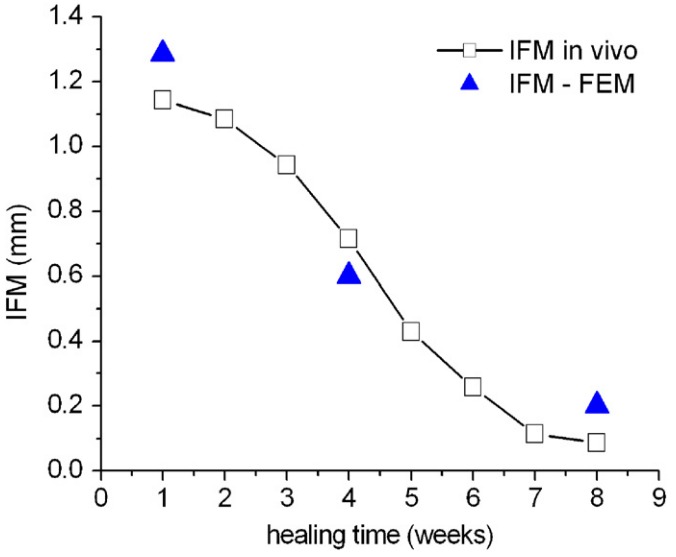

Fig. 4. Comparison between the FEM simulation and in vivo animal study of inter-fragmentary movement (IFM) [21].

2.3. BEM simulation in a bony poroelastic media

As a rough simplification of actual trends in bone healing simulation, a linear-elastic analysis was used to simulate the stimulatory and inhibitory effects of strains and local stresses on the tissue differentiation process.

Subsequently, the pore pressure was included into a stationary-poroelastic callus model, as a part of the stimuli function. These boundary element (BEM) analyses allowed us to extend the observations made by other authors and a new correlation is proposed. In addition to earlier quantitative theories, recent poroelastic models will be able to compare the tissue properties evolution completely, such as the elastic moduli (E) and Poisson ratio (υ), depending on both strain and pore pressure fields.

It is now clear that other factors influence the bone healing pattern, but the underlying hypothesis in this work is that a combination of local strain and pore pressure are the only stimuli to be considered.

The analytical kernels shown in Eq. (3) and their asymptotic behavior were taken from BEM quasi-static axi-symmetric thermoelastic approach [12,15,16,19,20,32].

Dargush and Banerjee [33] also show a detailed analysis of the poroelastic steady-state components of the fundamental solutions, showing the strong analogy between uncoupled termoelasticity and poroelasticity, asuming the corresponding poroelastic constants.

The kernels were implemented into a multi-zone, stationary–spatial boundary element framework for 3D elastic and potential problems available in Beer [8]. In particular, the singular terms appearing in the axi-symmetric boundary integral equations have been calculated using a mixed scheme for numeric and analytical integration. The analytical treatment follows a new methodology proposed by Graciani et al. [34] for continuous linear elements. This methodology include the asymptotic expansions of the fundamental solution of the displacements and tractions (see Eqs. (4) and (5)), allowing the calculation when the collocation point belongs to one element by the analytical integration of the singular terms and the numerical integration of the regular subtracted fundamental solutions.

$$U^{*}_{\alpha\eta}(P,Q) = U^{w}_{\alpha\eta}\ln(\varepsilon) + U^{B}_{\alpha\eta}[P,\tau(Q)]\varepsilon\ln(\varepsilon) + O[1] \tag{4}$$

$$T^{*}_{\alpha\eta}(P,Q) = \frac{T^{s}_{\alpha\eta}[\tau(Q),n(Q)]}{\varepsilon} + T^{w}_{\alpha\eta}[P,n(Q)]\ln(\varepsilon) + T^{B}_{\alpha\eta}[P,\tau(Q),n(Q)]\varepsilon\ln(\varepsilon) + O[1] \tag{5}$$

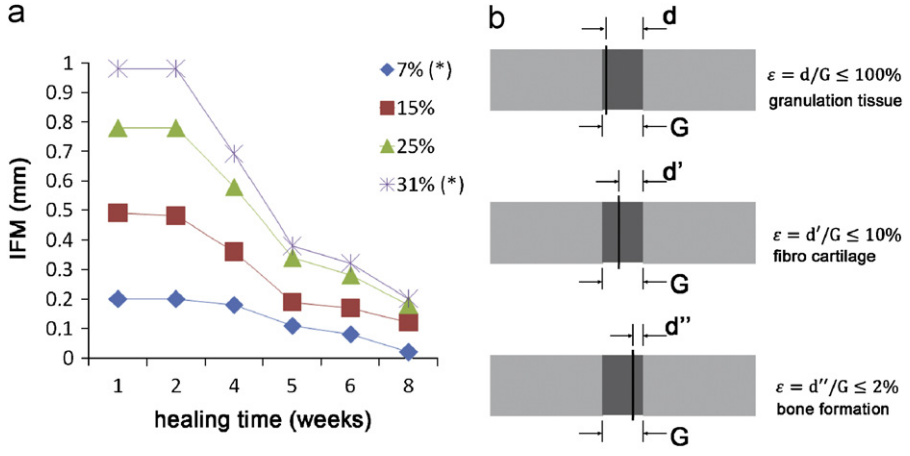

Fig. 5. (a) Relationship between IFMs history and IFS [28], (b) Perren IFS theory [31]. (*) Claes et al. [30].

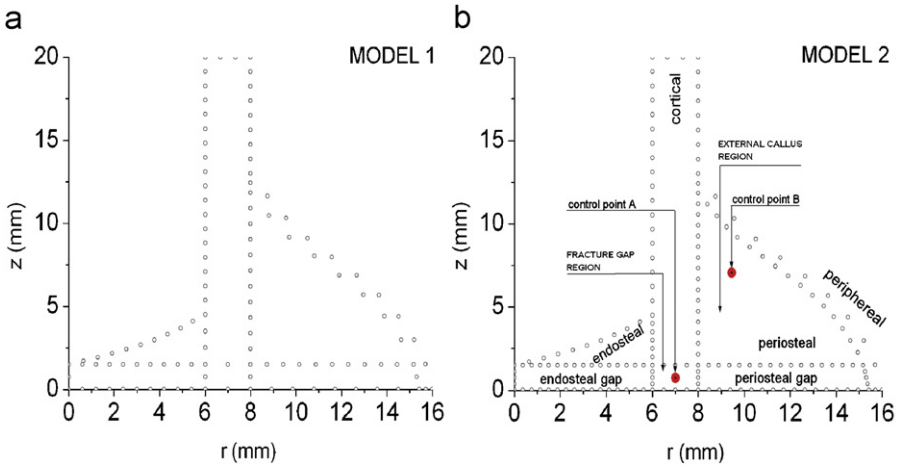

Fig. 6. Sensitivity analysis performed to validate the axi-symmetric integral formulation for elasticity: (a) first model within 177 elements and (b) second model within 267 elements. The third and fourth model had 467 and 1107 elements, respectively. The control points were placed in regions with high strain expected.

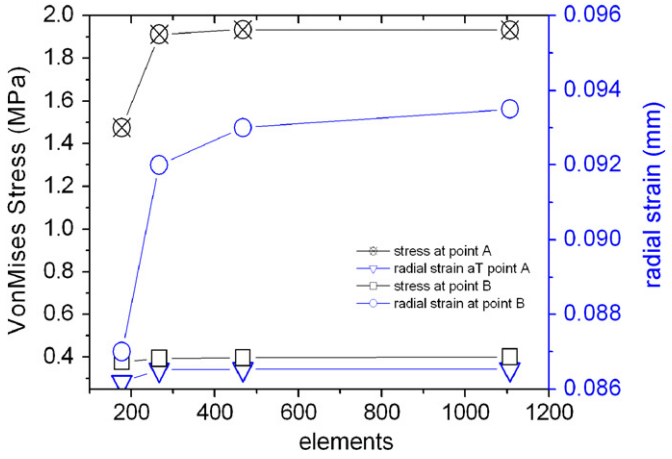

Fig. 7. Convergence in the solution of the four models considered.

being τ and n the unit tangent and outward normal to the boundary at Q.

Some numerical examples help to validate the implementation process. First, the axi-symmetric integral formulation for elasticity was tested comparing results with well known analytical solutions of elastic problems, followed by the accuracy analysis of the thermoelastic kernels assembling using a similar procedure. Once the thermoelastic code was accomplished, the substitution of appropriate poroelastic constants is carried out and a new validation is performed [35].

The next section shows two examples of the validation process. Based on the prescribed boundary conditions and the small range of allowed axial strain, a previous mesh refinement for sensitivity analysis was performed using the Hooke's law and an axi-symmetric boundary element model was generated for each stage (see Figs. 6 and 7). All boundary regions and a representative number of internal points were included into the models. Isoparametric linear elements were used, according to the methodology proposed by Graciani et al. [34].

Once the method proposed was tested [19], the uncoupled Biot linear consolidation theory [13] was implemented to simulate the tissue differentiation process.

In this simulation, the phenotype of 3 mm fracture gap size was studied. Once again symmetric boundary conditions are assumed, the axial displacements of the nodes on the r-axis were constrained, while, the nodes on the z-axis were restricted in the radial direction. Additionally, fluid flow was also set to zero in those cases and both the solid and the fluid constituents were modeled as compressible with the material properties shown in Table 2.

As a consequence of using the uncoupled poroelasticity, additional boundary condition (θ) is needed for the diffusive pore pressure problem. This data was taken from Claes and Heigele [21] and play an important role in strains/stresses calculation.

According to the results shown in Fig. 7, the third model was chosen to represent the behavior of the new field variables.

As an example of the thermoelastic code capability to obtain appropriate results, the analysis of the hollow cylinder subjected to a distributed uniform loading and constant temperature in the inner surface is shown (Fig. 8).

A BEM model using 48 linear elements was used to calculated the radial displacement u_r (Fig. 9a) as well as, the stresses (Fig. 9b) in the radial and tangential direction (S_{11} and S_{22}).

The results reported by all numerical studies shown that the boundary element framework is an accurate alternative to describe in a simplified form the tissue response during bone healing process.

As mentioned before, a loading of 500N and 31% of IFS were considered to impose a prescribed displacement at the top of cortical region, according to the healing time (Fig. 5a).

Initially, the entire callus was assumed to consist of granulation tissue (see Fig. 6a). The ossification path (Fig. 3A.a) was attached to the periosteal surface of the bone, where the precursor cells could migrate [36,37]. The periosteum is supposed to be intact; therefore the fracture is more stable from the beginning [29]. The second model (Fig. 10b) contained manly callus of intermediate stiffness in a small region along the periosteum, and soft callus tissue adjacent to it. In the third model, the callus tissue was characterized by five tissue types: granulation tissue, soft callus, intermediate callus, stiff callus and chondroid ossification zone (see Fig. 10c).

Instead of explicitly modeling cell migration and proliferation, the effects of cells activity on tissue properties and spatial distribution were associated to each healing stage supported by in vivo animal observations [30] (see Table 1). Additionally new poroelastic variables were added (see Table 2), according to the properties reported by Isaksson et al. [22] and Lacroix and Prendergast [36].

Table 2
Poroelastic properties: E (Young's modulus), v (drained Poisson's ratio), K_s (drained modulus), K_f (undrained modulus), ϕ (porosity), k (hydraulic permeability; $\kappa = k/\mu$), v_u (undrained Poisson's ratio), B (Skempton's modulus).

Tissue type	E^a (MPa)	v^a	K_s^b (MPa)	K_f^b (MP)	ϕ^b	K^b (m^4/Ns)	$v_u{}^c$	B^c
Initial connective tissue (ICT)	3	0.4	2 300	2300	0.8	1.0×10^{-14}	0.5	0.998
Soft callus (SOC)	1000	0.3	3 400	2300	0.8	5.0×10^{-15}	0.428	0.889
Intermediate stiffness callus (MSC)	3000	0.3	17 660	2300	0.8	1.0×10^{-13}	0.384	0.53
Stiff callus (SC)	6000	0.3	17 660	2300	0.8	3.7×10^{-13}	0.341	0.321
Chondroid ossification zone (COZ)	10,000	0.3	13 920	2300	0.8	3.7×10^{-13}	0.316	0.177
Cortex (C)	20,000	0.3	17 660	2300	0.04	1.0×10^{-17}	0.302	0.182
Fascie (F)	250	0.4	2 300	2300	0.8	1.0×10^{-14}	0.482	0.949

[a] Claes and Heigele [21].
[b] Isaksson et al. [22].
[c] Calculated using constitutive law.

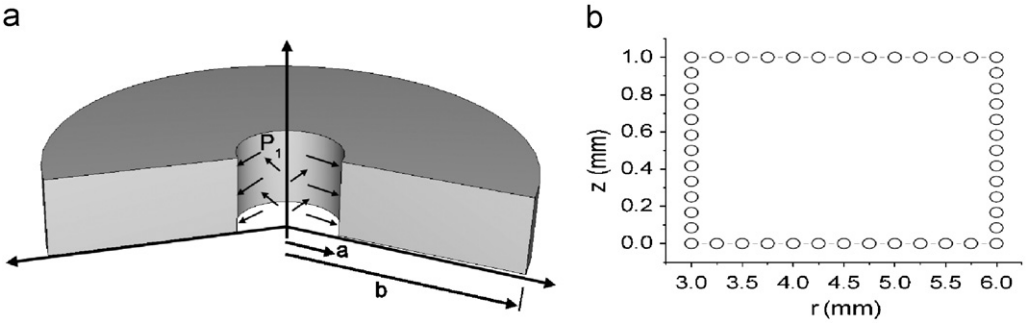

Fig. 8. Hollow cylinder problem: (a) 3D thermoelastic problem and (b) shape discretization using 48 linear elements.

3. Poroelastic results

3.1. Inter-fragmentary motion

For each model, both the IFM and IFS were calculated (see Fig. 11). The IFS was obtained following the Perren theory (see Fig. 5b).

3.2. Global strain field and pore pressure

Fig. 12 shows the global results obtained in this work for strains and pore pressure fields, in three specific stages of the consolidation process. The effect of the Skempton pore pressure coefficient was considered.

3.3. Pore pressure along the ossification path

This section shows the calculated pore pressures (Ph) along the ossification paths (see Fig. 13). The origin was taken close to the periosteal surface as depicted in Fig. 3A. The results are presented illustrating the type of ossification (OI/OE) for each stage considered.

4. Discussion

All models were discretized using isoparametric continuous linear elements taking advantage from a boundary element approach, in spite of the number of elements needed when quadratic elements are used. The number of internal points was set to 40 per region leading to better mapping of the results.

A quasi-static BEM poroelastic analysis was carried out considering the same boundary conditions used in a previous elastic analysis (prescribed displacements mostly, see Fig. 10) and introducing a new variable, the pore pressure.

Since the uncoupled poroelasticity formulation has been applied, the pore pressure magnitudes for prescribed conditions were obtained directly from the Claes and Heigele model. This implies that equilibrium between pore and the surrounding environment has not been reached and changes in pressure values can be expected.

In the first stage, the simulation begins with granulation tissue (post-inflammation phase) and finishes with boundary regions related with every tissue-type considered at 8 weeks. Most cellular events were not included directly.

For three stages considered (1, 4 and 8 weeks), the results shows accuracy under static and stationary conditions. Our results regarding the global strain and pore pressure field correlate well with observations discussed by Cowin [17].

Some differences between the poroelastic stimuli and the original quantitative theory were found, especially from the fourth week and beyond. The first stage shows strain magnitudes almost constants along the ossification path and bigger than those reported by Claes and Heigele [21]. The pore pressures were high at the beginning where a progressive volume expansion associated with the migration and differentiation of the osteoprogenitor cells is taking place. These values become moderate through healing time due to the increasing of tissue stiffness. This behavior was also

predicted by Lacroix et al. [1] and Lacroix and Prendergast [36] showing high shear strain values and fluid flow adjacent to the origin of the ossification path. The flow in this point is believed to be associated with negative pressures depicted in Fig. 13.

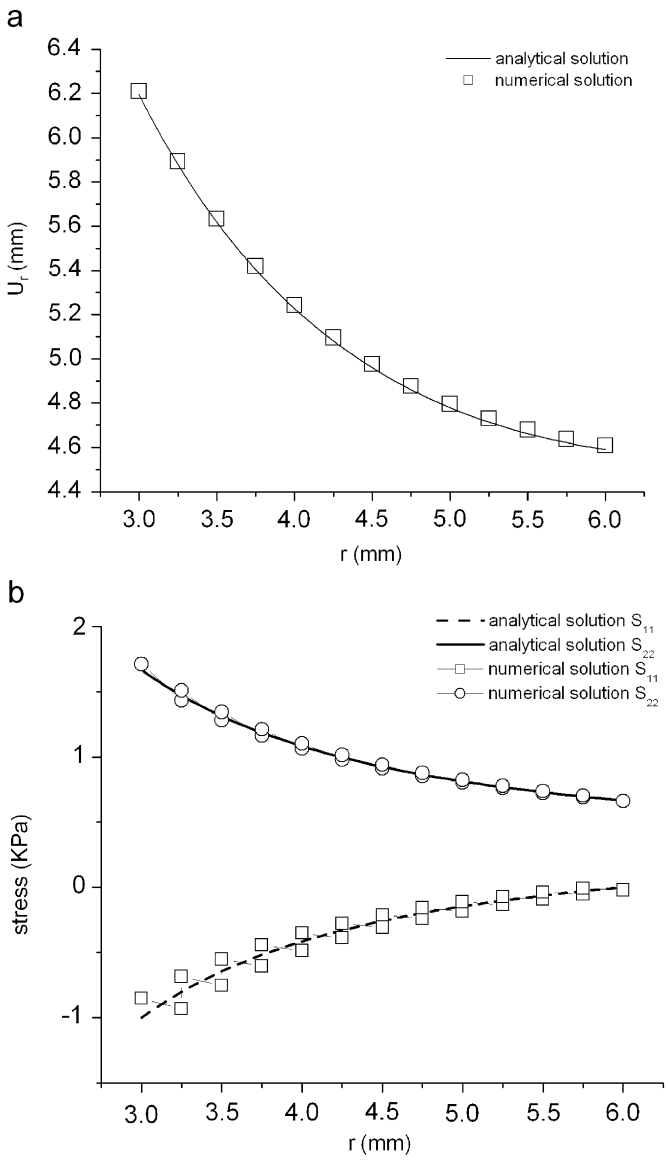

Fig. 9. (a) Hollow cylinder problem. Radial displacement as a function of radius. (b) Hollow cylinder problem. The picture shows a comparison between numerical and analytical results.

Using pore pressure as a part of differentiation signal, the first stage simulation established conditions to promote ossification around the periosteum and in the major part of the endosteum area: moderate pressures and high magnitudes of strains as

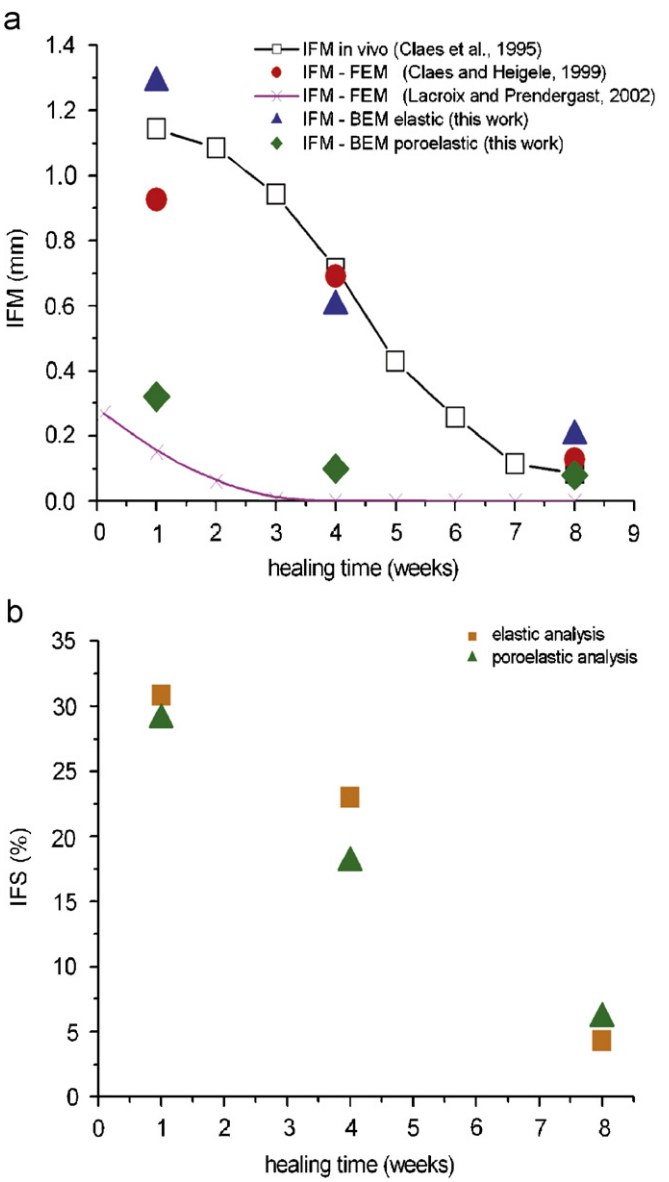

Fig. 11. (a) Comparison of IFMs calculated through in vivo, FEM and BEM analyses and (b) comparison of IFSs calculated through FEM and BEM analyses.

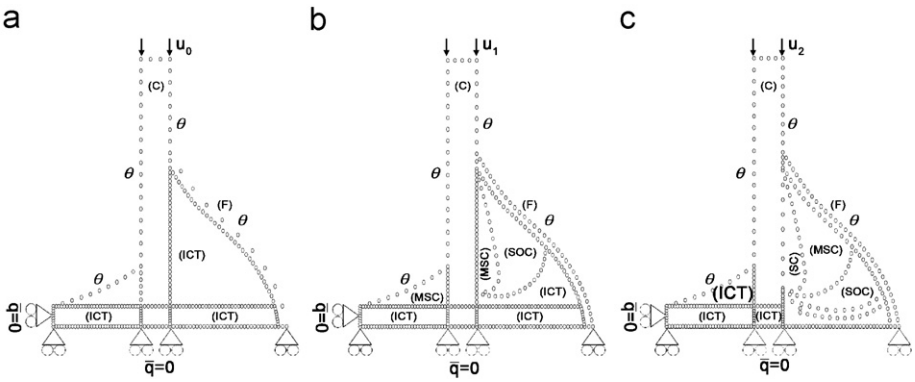

Fig. 10. Axi-symmetric bifasic boundary conditions at three healing stages: (a) 1 week, (b) 4 weeks and (c) 8 weeks.

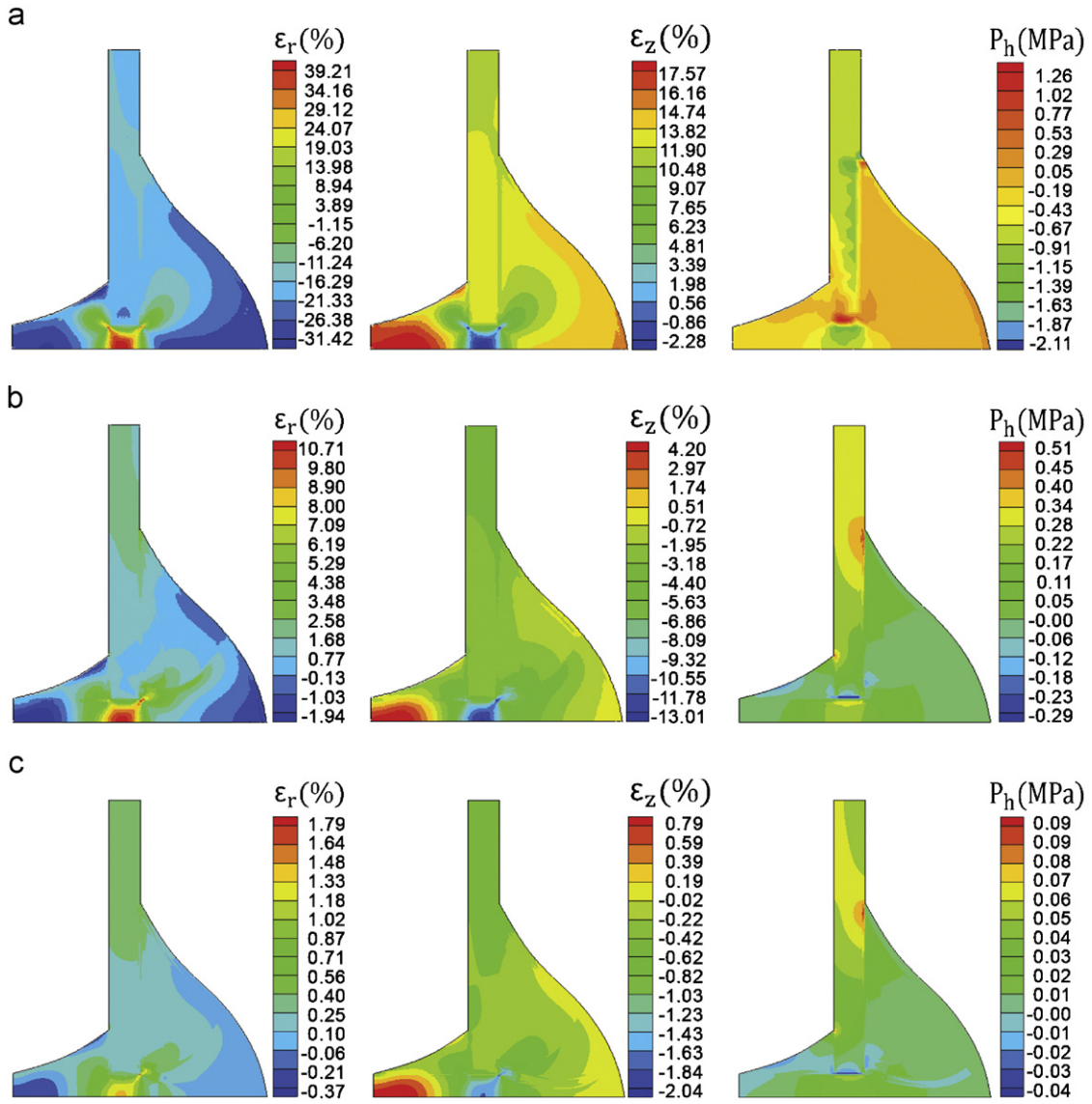

Fig. 12. Global distribution of strain in both radial and axial direction and pore pressure field. (a) First healing stage (1 week), (b) second healing stage (4 weeks) and (c) third healing stage (8 weeks). As described by Claes and Heigele [21], negative strain means a reduction and positive strain means an increase. The negative pore pressure implies a reduction of the volume and positive values an expansion.

depicted in Figs. 12a and 13. The cortical gap exhibits high pressures under compression, stimulating bone formation by endochondral process (see Fig. 12a). These values become moderated toward the periosteal gap, where granulation tissue is mostly found.

In the beginning of the fourth week, the pressures along the new ossification path behave differently compared with the hydrostatic pressures reported by Claes and Heigele [21]. Notice the increasing of the pressure values as we get closer to the periphereal callus area (see Fig. 13). At this point, a matrix formed by cartilage is mainly seen due to endochondral ossification progress [36]. However, the magnitudes of strains (absolute value) were small enough to stimulate the formation of cartilaginous tissue. Later, the cell differentiation process continues toward osteoclasts mostly and a new volume expansion proceeds. As the endochondral and intramembranous ossification paths find each other (stage 2 and 3) and new tissues are formed, the strains become lower (Fig. 12c) and the pore pressure field tends to equilibrium progressively (Fig. 13).

On the other hand, the IFM was also sensitive to the constitutive law and did not reproduce the in vivo measurements (see Fig. 7a). However, the findings were according to the range (0.2–1n) proposed to be optimal for fracture healing [18,24].

Lacroix and Prendergast [36] also studied the IFM as a function of boundary conditions and time healing. They showed similar values of IFM (Fig. 11a). The differences are mostly due to the material properties used.

When the pore pressure becomes lower (equilibrium), large stiffness is commonly found in the gap site resulting in small axial movements, as a consequence, the IFS is more and more dependent of the solid matrix behavior (Fig. 11b).

Using only poroelasticity, the hypothesis that the amounts of strain and hydrostatic stresses along existing calcified surfaces control the differentiation of tissues is confirmed once again. Therefore, the implementation of the numerical framework proposed works well under some simplifications.

As we know, the Claes and Heigele tissue differentiation theory is typically referenced in most of the recent poroelastic mechano-regulation algorithms [2,18,29], but only in a qualitative way, mainly by the constitutive laws applied and the differences between properties magnitudes.

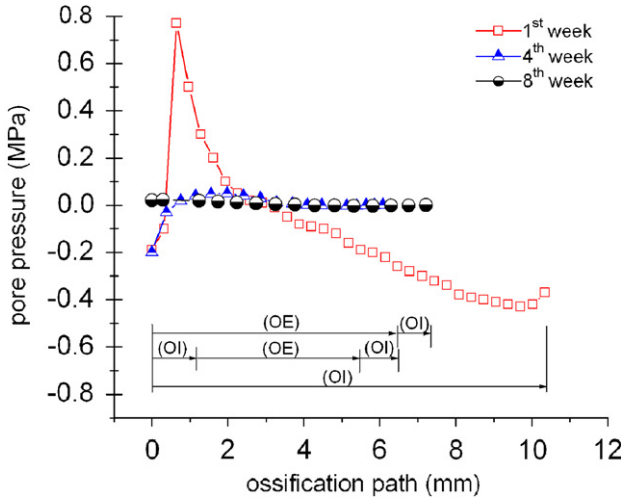

Fig. 13. Stress poroelastic results along bony surfaces using boundary element method. (OI) Surface of intramembranous ossification, (OE) surface of endochondral ossification.

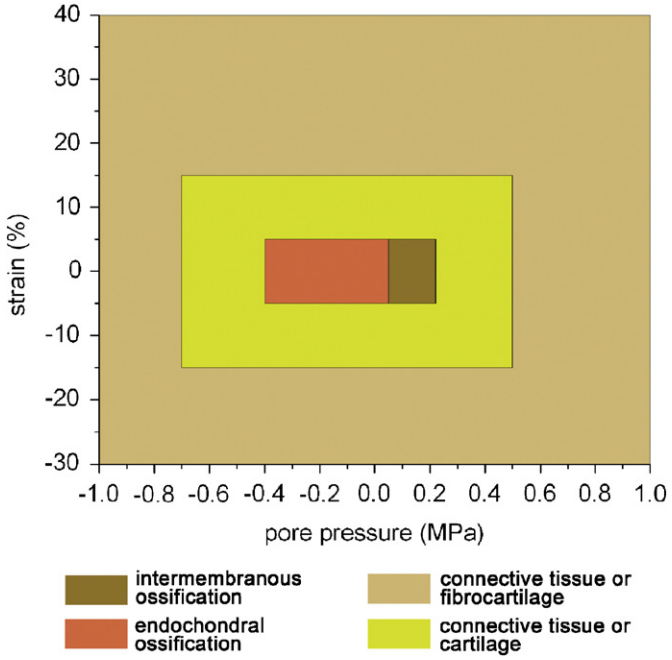

Fig. 14. New correlation between poroelastic mechanical conditions and tissue types. Cartilaginous tissue was incorporated according to the Lacroix and Prendergast's findings.

On the other hand, those models usually study most cellular events thoroughly, even if there is not emphasis showing the evolution of material properties (Young modulus, Poisson ratio, etc.).

Based on poroelastic-only constitutive law, a new correlation is proposed (Fig. 14) and a direct quantitative comparison of the mechanical environment is now possible allowing a better understanding of the results reported by previous FEM simulations. The basic procedure was to evaluate mainly the postprocessing BEM data along the ossification patterns for each stage considered, and to observe how those magnitudes defined new ranges for each tissue-type according with the assumed hypothesis. The adjacent areas were also studied.

This correlation also could help to test indirectly the assumed relations for material properties evolution, checking the magnitudes step-by-step and their influences on the mechanical tensors reported by any numerical framework.

5. Concluding remarks

This work represents an important contribution in the application of boundary element method for biological problems. In particular, the capability for bone healing axi-symmetric simulation in a poroelastic media to establish the mechanical environment during tissue differentiation process has been demonstrated.

Finite element and finite difference methods are widely applied to these kind of problems. However, most of the fundamental solutions and alternative boundary formulations are available and complex simulations like bone healing are believed to be carried out successfully based on BEM analysis. From this point of view, BEM can be seen as an attractive tool for external shape remodeling. The authors also want to highlight the effort involved in preparing BEM algorithms for modeling tissue regeneration according to recent mechano-regulation theories. Nevertheless, complex models can be implemented into a BEM framework by using the results obtained in this work.

Is well known that the process of cell differentiation into specialized cells responsible for producing the different tissues involved in the bone regeneration (hematoma, connective tissue, cartilage, etc.), that the movement of the callus boundary that exhibits non-linear and non-homogeneous anisotropic behavior, and that the boundary conditions and geometry are not axially symmetric. This implies that the application of a generalized poroelastic boundary integral equation for homogeneous isotropic media is a key simplification in this work. However, the multi-domain capability of the code allowed handling the change of material properties in a simplified manner considering the homogeneity by region.

Using a boundary framework we have characterized the phenotype tissues involved into bone healing. The poroelastic study allowed to extend the observations made by Claes and Heigele [21] and a new poroelastic-only correlation is proposed. Although the first results are promising, it is necessary to evaluate this correlation with other experimental results.

The need to include transitory kernels into the boundary integral formulation, as well as the cell diffusion analysis and moving boundary techniques is a key aspect for future dynamic applications.

Acknowledgements

The authors would like to thanks to Prof. Adrián Cisilino, Universidad Nacional de Mar del Plata (Mar del Plata–Argentina), Prof. Enrique Graciani, Universidad de Sevilla (Sevilla–Spain) and to Prof. Gernot Beer for giving permission to use the BEM code.

As well, financial support for this work was provided by:

- ALFA project II-0357-FA-FCD-FI (ELBEnet), European Community.
- Consejo de Desarrollo Científico y Humanístico (CDCH), Universidad Central de Venezuela, Venezuela.
- Fondo Nacional de Ciencia, Tecnología e Innovación (FONACIT), Venezuela.

References

[1] Lacroix D, Prendergast PJ, Li G, Marsh D. Biomechanical model to simulate tissue differentiation and bone regeneration: application to fracture healing. Med Biol Eng Comput 2002;40:14–21.
[2] Doblaré M, García JM, Gómez MJ. Modeling bone tissue fracture and healing: a review. J Eng Fract Mech 2004;71:1809–40.
[3] Caplan AI, Boyan BD. Endochondral bone formation: the lineage cascade. In: Mechanism of bone development and growth. FL: CRC Press; 1994.

[4] Einhorn TA. The cell and molecular biology of fracture healing. Clin Orthop Rel Res 1998;355:S7–S21.
[5] Aliabadi F. The boundary element method: applications in solids and structures. England: Wiley; 2002.
[6] Annicchiarico W, Martínez G, Cerrolaza M. Boundary elements and β-spline surface modeling for medical applications. J Appl Math Model 2007;31(2): 194–208.
[7] Martínez G, García JM, Doblaré M, Cerrolaza M. External bone remodeling through boundary elements and damage mechanics. J Math Comput Simul 2006;73:183–99.
[8] Beer G. Programming the boundary element method: an introduction for engineers. UK: Wiley; 2001.
[9] Divo E, Kassab AJ. A generalized boundary integral equation for axisymmetric isotropic media. In: Proceedings of the XIX international conference on the boundary element method 1997, p. 453–62.
[10] Cheng AHD, Cheng DT. Heritage and early history of the boundary element method. Eng Anal Boundary Elem 2005;29:268–302.
[11] Zerroukat M, Power H, Wrobel LC. Heat and solute diffusion with a moving interface: a boundary element approach. Int J Heat Mass Transfer 1998; 41(16):2429–36.
[12] Qiu ZH, Wrobel LC, Power H. Boundary element approach to mass and charge transport in electrochemical cells. Eng Anal Boundary Elem 1995;15: 299–312.
[13] Brebbia CA, Dominguez J. Boundary element: an introductory course. UK: Computational Mechanics Publications; 2003.
[14] Biot MA. General solutions of equations of elasticity and consolidation for a porous material. J Appl Mech 1956;78:91–6.
[15] Dargush GF, Banerjee PK. Time dependent axisymmetric thermoelastic boundary element analysis. Int J Numer Meth Eng 1992;33:695–717.
[16] Balas J, Slâdek V, Slâdek. Stress analysis by boundary element method. 1st ed. Amsterdam: Elsevier; 1989.
[17] Cowin SC. Bone mechanics handbook. FL: CRC Press LLC; 2001.
[18] Epari DR, Taylor WR, Heller MO, Duda GN. Mechanical conditions in the initial phase of bone healing. Clin Biomech 2006;21:646–55.
[19] Bakr AA, Fenner RT. Boundary integral equation analysis of axisymmetric thermoelastic problems. J Strain Anal 1983;18(4):239–51.
[20] Banerjee PK. The boundary element method in engineering. 2nd ed. UK: McGraw-Hill International; 1994.
[21] Claes LE, Heigele CA. Magnitudes of local stress and strain along bony surfaces predict the course and type of fracture healing. J Biomech 1999;32:255–66.
[22] Isaksson H, Wilson W, Van Donkelaar CC, Huiskes R, Ito K. Comparison of biophysical stimuli for mechano-regulation of tissue differentiation during fracture healing. J Biomech 2006;39:1507–16.
[23] Augat P, Claes L. Quantitative assessment of experimental fracture repair by peripheral computed tomography. Calcif Tissue Int 1997;60:194–9.
[24] Duda GN, Kirchner H, Wilke H-J, Claes L. A method to determine the 3-D stiffness of fracture fixation devices and its application to predict inter-fragmentary movement. J Biomech 1998;31:247–52.
[25] Claes LE, Heigele CA, Neidlinger-Wilke C, Kaspar D, Seidl W, Margevicius KJ, et al. Effects of mechanical factors on the fracture healing process. Clin Orthop 1998;355:S132–47.
[26] Augat P, Burger J, Schorlemmer S, Henke T, Peraus M, Claes L. Shear movement at the fracture site delays healing in a diaphyseal fracture model. J Orthop Res 2003;21:1011–7.
[27] Klein P, Schell H, Streitparth F, Heller M, Kassi JP, Kandziora F, et al. The initial phase of fracture healing is specifically sensitive to mechanical conditions. J Orthop Res 2003;21:662–9.
[28] García-Aznar JM, Kuiper JH, Gómez-Benito MJ, Doblaré M, Richardson J. Computational simulation of fracture healing: Influence of inter-fragmentary movement on the callus growth. J Biomech 2007;40(7): 1467–76.
[29] Gómez-Benito MJ, García-Aznar JM, Kuiper JH, Doblaré M. Influence of fracture gap size on the pattern of long bone healing: a computational study. J Theor Biol 2005;235(1):105–19.
[30] Claes L, Augat P, Wilke HJ. Influence of size and stability of the osteotomy gap on the success of fracture healing. J Orthop Res 1997;15(4):577–84.
[31] Chao EYS, Inoue N. Biophysical stimulation of bone fracture repair, regeneration and remodeling. Eur Cells Mater 2003;6:72–85.
[32] De lacerda LA, Wrobel LC. Frictional contact analysis of coated axisymmetric bodies using the boundary element method. J Strain Anal 2000;35(5):423–40.
[33] Dargush GF, Banerjee PK. A boundary element method for axisymmetric soil consolidation. Int J Solids Struct 1991;28:897–915.
[34] Graciani E, Mantic V, Paris F, Blazquez A. Weak formulation of axisymmetric frictionless contact problems with boundary elements application to interface cracks. J Comp Estruc 2005;83:836–55.
[35] González Y, González C, Cerrolaza M. Modeling bone healing by boundary element method. Rev Int Métodos Numéricos para Cálculo y Diseño en Ingeniería 2008;24(2):115–36 [in Spanish].
[36] Lacroix D, Prendergast PJ. A mechano-regulation model of tissue differentiation during fracture healing: analysis of gap size and loading. J Biomech 2002;35:1163–71.
[37] Gerstenfeld LC, Cullinane DM, Barnes GL, Graves DT, Einhorn TA. Fracture healing as a post-natal development process: molecular, spatial, and temporal aspects of its regulation. J Cell Biochem 2003;88:873–84.

Glossary

Healing: is the process by which the cells in the body regenerate and repair to reduce the size of a damaged or necrotic area.
Extracellular matrix: is the major constituent of bone, surrounding the cells.
Inflammatory cells: group formed mostly by growth factors and other cytokines.
Mesenchymal cells: are multipotent stem cells that can differentiate into a variety of cell types including osteoblasts, chondrocytes and myocytes.
Angioblasts: the embryonic mesenchymal tissue from which blood cells and blood vessels arise.
Fibroblasts: is a type of cell that synthesizes and maintains the extracellular matrix of many animal tissues.
Chondroblasts: is a cell which originates from a mesenchymal stem cell and forms chondrocytes, commonly known as cartilage cells.
Osteoblasts: is a mononucleate cell that is responsible for bone formation.
Woven bone: is a disorganized structure with a high proportion of osteocytes deposited in young and in healing injuries.
Bone tissue: bone tissue is a specialized form of connective tissue and is the main element of the skeletal tissues.
Connective tissue: as the name implies, connective tissue serves a ''connecting'' function. It supports and binds other tissues.
Granulation tissue: is the perfused, fibrous connective tissue that replaces a fibrin clot in healing wounds.
Cartilage: is a type of dense connective tissue. It is composed of specialized cells called chondrocytes.
Bone remodeling: is a life-long process where old bone is removed from the skeleton (a sub-process called bone resorption) and new bone is added (a sub-process called bone formation). These processes also control the reshaping or replacement of bone during growth and following injuries.
Bone fracture: is a medical condition in which a bone is cracked or broken. It is a break in the continuity of the bone.
Bone callus: is a temporary formation of fibroblasts and chondroblasts which forms at the area of a bone fracture as the bone attempts to heal itself.
Endochondral ossification: is the cartilage differentiation processes that lead to skeletal formation.
Intramembranous ossification: formation of bone tissue directly from connective tissue without a preliminary cartilage stage.
Chondrogenesis: chondrogenesis and endochondral ossification are the cartilage differentiation processes that lead to skeletal formation, as well as skeletal repair in the adult.
Osteogenesis: process involving formation of new bone.
Ossification: is the process of bone formation, in which connective tissues, such as cartilage are turned to bone or bone-like tissue.
Periosteum: is a membrane that lines the outer surface of all bones, except at the joints of long bones. Periosteum consists of the irregular type of dense connective tissue.
Endosteum: is a thin layer of connective tissue which lines the surface of the bony tissue that forms the medullary cavity of long bones.